



1 **Influence of Tropospheric Temperature on the Formation and Aging of
2 Secondary Organic Aerosol from Biogenic Vapor Mixtures**

3 *Linyu Gao^{1,2,*}, Stella E. I. Manavi³, Claudia Mohr^{4,5}, Junwei Song^{1,2}, Cheng Wu⁶, Thomas
4 Leisner^{1,7}, Spyros N. Pandis³, and Harald Saathoff^{*}*

5 ¹ Institute of Meteorology and Climate Research, Karlsruhe Institute of Technology, Karlsruhe,
6 76344, Germany

7 ² Now at: Université Claude Bernard Lyon 1, CNRS, IRCELYON, Villeurbanne, 69626, France

8 ³ Department of Chemical Engineering, University of Patras, Patras, 26504, Greece

9 ⁴ Department of Environmental Systems Science, ETH, Zurich, 8092, Switzerland

10 ⁵ PSI Center for Energy and Environmental Sciences, Paul Scherrer Institute, Villigen, 5232,
11 Switzerland

12 ⁶ Department of Chemistry and Molecular Biology, University of Gothenburg, 41296,
13 Gothenburg, Sweden

14 ⁷ Institute of Environmental Physics, Heidelberg University, Heidelberg, 69120, Germany

15 Correspondence to: Linyu Gao (linyugao@163.com) & Harald Saathoff
16 (harald.saathoff@kit.edu)

18

19 **Abstract**

20 Atmospheric temperature and composition variations significantly influence secondary organic
21 aerosol (SOA) formation and aging, and thus fine particulate matter levels and properties
22 relevant for climate, air quality, and human health. However, the temperature dependence of
23 SOA formation and aging from mixed volatile organic compounds (VOCs) remains
24 insufficiently understood. Therefore, we investigated SOA formation from the oxidation of
25 isoprene and α -pinene mixtures covering the range of tropospheric temperatures (213 – 313 K).
26 We further examine the aging of the resulting SOA by gradually warming to mimic their
27 atmospheric transport and diurnal aging processes. Notably, at 213 K, isoprene most strongly
28 suppresses α -pinene dimer (C_{18-20}) formation, with isoprene- α -pinene cross dimers appearing
29 3.5 times more frequently than at 273 K, while the suppression is not temperature-sensitive
30 above 273 K. Upon subsequent warming, particles formed at different temperature ranges
31 undergo distinct aging processes including aerosol evaporation and water uptake. Surprisingly,
32 particles formed at higher temperatures are more oxidized yet more volatile than those formed
33 at lower temperatures and subsequently warmed. Chemical transport modeling accounting for
34 temperature-depended simultaneous oxidation of isoprene and α -pinene predicts higher SOA
35 levels across Europe, aligning more closely with observations. These findings highlight the
36 need to consider both temperature and the interaction of biogenic VOCs to accurately describe
37 SOA formation, aging, and global burden.



38 1. Introduction

39 Aerosol particles are ubiquitous in the atmosphere, significantly impacting climate and having
40 adverse effects on air quality and human health (Paasonen et al., 2013; Mahowald, 2011; Aubry
41 et al., 2021). Organic aerosol (OA) makes up 20-90 % of the total fine particulate mass in the
42 troposphere (Jimenez et al., 2009). An important contributor to the global OA burden is
43 secondary organic aerosol (SOA), which emerges from the condensation of organic compounds
44 formed by the oxidation of volatile organic compounds (VOCs) (Kroll and Seinfeld, 2008).
45 Generally, the key precursors for global SOA are biogenic VOCs, of which isoprene (C_5H_8)
46 and monoterpenes ($C_{10}H_{16}$) are the most abundant (Kanakidou et al., 2005). Consequently, large
47 efforts (Kanakidou et al., 2005; Carlton et al., 2009; Kroll and Seinfeld, 2008; Zhang et al.,
48 2015; Hallquist et al., 2009; Lopez-Hilfiker et al., 2014; McFiggans et al., 2019; Takeuchi et al.,
49 2022) have been put into investigating their formation chemistry and particle physicochemical
50 properties of biogenic SOA.

51 Most of these studies were done at or near room temperature (Zhang et al., 2015; Lopez-Hilfiker
52 et al., 2015; Kourtchev et al., 2015; Takeuchi et al., 2022; McFiggans et al., 2019). The
53 troposphere however covers a wide temperature range between 310 K to 200 K. In the near-
54 surface atmosphere, VOCs can be oxidized at varying ambient temperatures throughout the day,
55 depending on the season and region. By convective systems, VOCs could reach to higher
56 altitudes where they can be oxidized at lower temperatures (Schulz et al., 2018; Liu et al., 2023).
57 This is important for the prediction of SOA levels especially in the free troposphere.
58 Temperature affects the reaction rates and pathways (Bilde et al., 2015; Bianchi et al., 2019) of
59 VOCs oxidation as well as the gas-to-particle partitioning of oxidation products (Sheehan and
60 Bowman, 2001; Donahue et al., 2006; Jonsson et al., 2008; Simon et al., 2020), thereby altering
61 the formation, chemical composition, and physicochemical properties of aerosol particles. Thus,
62 developing a comprehensive study covering tropospheric conditions is essential for
63 understanding SOA formation and aging processes in the real atmosphere.

64 Isoprene makes up the largest portion of the global biogenic VOC emissions (Owen et al., 2003;
65 Sindelarova et al., 2014), making it an important SOA precursor despite its relatively low
66 individual mass yield of <5% (Xu et al., 2014; Lamkaddam et al., 2021; Carlton et al., 2009).
67 Previously, Kiendler-Scharr et al. (2009) and McFiggans et al. (2019) found that at room
68 temperature, the presence of isoprene reduces SOA formation from the oxidation of α -pinene.
69 This is due to the competition of isoprene and α -pinene for reacting with hydroxyl radicals (OH)
70 (McFiggans et al., 2019) and the formation of more volatile C_{15} dimers from the reaction of C_{10}
71 peroxy radicals (RO_2) of α -pinene and $C_5 RO_2$ of isoprene, instead of less volatile C_{20} dimers
72 from self-reactions of $C_{10} RO_2$ from α -pinene alone. However, the temperature dependence of
73 RO_2 cross reactions in the isoprene and α -pinene systems as well as the effects of temperature
74 changes on SOA aging during atmospheric processes such as transport and diurnal aging
75 remains to be fully understood. This knowledge gap is critical given the varying atmospheric
76 abundances of these compounds across different ecosystems. For instance, in the Amazonian
77 rainforest, summertime isoprene mixing ratios range from 0.1 to 20 ppb (Yáñez-Serrano et al.,
78 2020; Yáñez-Serrano et al., 2018), while monoterpenes are typically below 1 ppb but can reach
79 up to 5.5 ppb. In contrast, European forests exhibit lower isoprene levels, typically below 1 ppb
80 but reaching up to ~5 ppb during warm daytime periods (Li et al., 2021; Petersen et al., 2023).
81 Monoterpene concentrations in these forests are also generally below 1 ppb but can reach
82 several tenths of ppb during summer across a typical temperature range of 10–35 °C (Li et al.,
83 2021). Therefore, investigating the impact of temperature on the oxidation of isoprene and α -



84 pinene mixtures at atmospherically relevant concentrations is essential to accurately predict
85 SOA formation in diverse environmental conditions (Tripathi et al., 2025; Curtius et al., 2024).

86 We thoroughly investigated the temperature-dependent formation and the properties of SOA
87 from the oxidation of the mixture of isoprene and α -pinene at 213 K (SOA_{213K}), 243 K
88 (SOA_{243K}), 273 K (SOA_{273K}), 298 K (SOA_{298K}), and 313 K (SOA_{313K}). The SOA formed at each
89 temperature was subsequently warmed with increments of 15–30 K over 10 hours to investigate
90 the aging processes (e.g., diurnal cycle) of SOA over a wider tropospheric temperature range
91 (i.e., SOA_{213K}–243K, SOA_{243K}–273K, SOA_{273K}–298K, and SOA_{298K}–313K). A series of cross dimers
92 from the two precursor VOCs were identified by making use of carbon isotope (¹³C) labelling
93 experiments, as well as by comparison with the sole α -pinene oxidation experiment. We
94 demonstrated the effect of temperature on the suppression of α -pinene dimers by isoprene and
95 the formation of two-precursor cross dimers. By studying the effect of warming on aged
96 particles, we distinguished the impact of temperature on both the chemistry and phase
97 partitioning of organic molecules and provided evidence that particles at different temperature
98 ranges undergo distinct aging processes (i.e., evaporation and water uptake) during warming.

99 **2. Methods**

100 **2.1 Simulation Chamber Experiments**

101 The data presented here was measured in two campaigns in 2019 (SOA19b) and 2021 (SOA21a)
102 covering 213 – 313 K in the Aerosol Interaction and Dynamics in the Atmosphere (AIDA)
103 aerosol and cloud simulation chamber at the Karlsruhe Institute of Technology (KIT). The
104 chamber is an 84.5 m³ aluminium vessel equipped with a LED solar radiation simulator and
105 with precisely controlled temperature, humidity, and gas mixtures. A fan allows all components
106 to be mixed well within 90 seconds (Saathoff et al., 2009). Details about the AIDA chamber
107 are given by previous studies (Möhler et al., 2003; Vallon et al., 2022; Wagner et al., 2006).

108 Two types of SOA were generated in batch mode from dark oxidation of: (1) sole α -pinene at
109 273 K (SOA_{ap-273}), (2) isoprene mixed with α -pinene at 213K, 243K, 273K, 298K, and 313K
110 (SOA_{213K}, SOA_{243K}, SOA_{273K}, SOA_{298K}, SOA_{313K}), respectively. The experimental conditions
111 are summarized in Table 1. Well defined amounts of isoprene and α -pinene were added to the
112 AIDA chamber with a flow of 10 L/min of synthetic air. Ozone was injected subsequently after
113 the biogenic VOC were mixed well inside the chamber, followed by the continuous addition of
114 tetramethyl ethylene (TME) generating OH radicals by its reaction with ozone. The OH
115 concentrations were $(0.8\text{--}1.5) \times 10^7$ molecules cm⁻³ in all experiments. The initial concentration
116 ratios of isoprene to α -pinene were kept at 1.0 ± 0.1 for all two-precursor experiments, while
117 the ratios of O₃ to α -pinene were 14 ± 3 among all experiments with the exception of Exp 1 at
118 213 K (O₃: α -pinene = 38). At 213 K, the initial concentration of isoprene and α -pinene was
119 separately injected by 6.7 ppb with O₃ in 253 ppb, followed by the second addition of two VOC
120 precursors by 13.5 ppb and the second injection of O₃ to 366 ppb. We note that the two times
121 of injections of precursors may have impact on the chemical regimes during the SOA formation
122 at 213 K compared to other experiments. Seed particles and OH scavengers were not used in
123 this work.

124 The initial reaction lasted 90 minutes, then the VOC precursors were depleted. The subsequent
125 course of the experiment consisted of one hour of photochemical aging by illumination and
126 then 14 hours of warming the entire chamber at a constant rate. The increment of temperature
127 before and after warming is shown in Table 1. To evaluate the effect of dilution, we injected



128 CO₂ which is a chemistry bystander before warming. The loss of CO₂ was less than 4% for all
129 experiments after 14 h of warming. Therefore, the dilution effect is neglectable.



130

Table 1. Experimental conditions for SOA from sole α -pinene and mixtures of isoprene and α -pinene.

Exp No.	SOA type		Initial formation	VOC conc. [ppb]		Temperature during warming (start → end) [K]	RH after warming [%]	Newly formed SOA conc. [$\mu\text{g m}^{-3}$]	Particle Yield
	Before warming	After warming		RH before warming [%]	O_3 [ppb]				
0	SOA _{ap-273}	-	273	63	20.5	0	345	-	65.3
1	SOA _{213K}	SOA _{213K → 243K}	213	16	20.2	20.2	347	213 → 243	4
2	SOA _{243K}	SOA _{243K → 273K}	243	80	25	25	367	243 → 273	6
3	SOA _{273K}	SOA _{273K → 298K}	273	58	21.5	20.8	371	273 → 298	12
4	SOA _{298K}	SOA _{298K → 313K}	298	28	31.3	28.6	355	298 → 313	10
5	SOA _{313K}	-	313	12	49.8	49.8	507	-	41.5
6	SOA _{ap-13C-isop-273}	-	273	61	20.8	23	353	273 → 298	0.09
7	SOA _{ap-13C-isop-298}	-	298	28	31.1	28	357	298 → 313	-



131 **2.2 Instrumentation**

132 The concentrations of VOC and semi-volatile organic particles were measured by a Proton-
133 Transfer-Reaction-Time-of-Flight-Mass-Spectrometer coupled with a Chemical Analysis of
134 Aerosol Online (CHARON-PTR-ToF-MS, Ionicon Analytik GmbH) particle inlet.

135 Bulk SOA was online detected by a high-resolution time-of-flight Aerosol Mass Spectrometer
136 (HR-AMS, Aerodyne Inc.), while the particle-phase chemical composition of SOA at molecular
137 level was detected by a chemical ionization mass spectrometer (CIMS) coupled with a filter
138 inlet for gas and aerosols (FIGAERO) using iodide (I^-) as reagent ions with 1 Hz time resolution
139 (Lopez-Hilfiker et al., 2014; Lee et al., 2014). The CIMS data presented in this work stems
140 from offline analysis. The filter samples were analyzed using a FIGAERO-iodide-CIMS. We
141 also note that the sensitivity of FIGAERO-iodide-CIMS is highly dependent on the
142 functionalities of the organic compounds and can vary by orders of magnitudes (Lopez-Hilfiker
143 et al., 2016; Lee et al., 2014; Riva et al., 2019). Therefore, the results shown in this work are
144 based on signal intensities but not mass concentrations. The detailed description of instruments,
145 filter sample collection, and data analysis are described in Section S1 and Figure S1.

146 O_3 was detected by a gas monitor (O_341M , Environment SA). Particle size distributions and
147 number concentrations were measured by a scanning mobility particle sizer (SMPS) utilizing a
148 differential mobility analyzer (DMA, 3071 TSI Inc.) connected to a condensation particle
149 counter (CPC, 3772, TSI Inc.). The total particle number concentrations were monitored by two
150 condensation particle counters (CPC, 3776 and 3022A, TSI Inc.).

151 Typically, background measurements for both gas and particle phase are done before and after
152 the addition of VOC to identify any contaminations inside the chamber. Gas background
153 confirms that there were no significant gas-phase contaminations for all the experiments. Most
154 of the particle background signals were coming from filter matrix contaminations mainly due
155 to fluorinated constituents of low relevance. Please note that the background in all experiments
156 was measured in the same way as described previously (Gao et al., 2022).

157 **2.3 SOA particle volatility determination**

158 The large number of organic compounds detected in the particle phase are presented in a one-
159 dimensional volatility basis set (1D-VBS) (Donahue et al., 2006), based on the effective
160 saturation concentration (C_{sat} , $\mu\text{g m}^{-3}$). In this work, 298 K C_{sat} ($C_{sat,298K}$, $\mu\text{g m}^{-3}$) values of
161 individual compounds are determined according to their measured elemental formulas applying
162 a parameterization using molecular corridors (Li et al., 2016). The saturation concentration of
163 species at other temperatures ($C_{sat,T}$, $\mu\text{g m}^{-3}$) can be derived from $C_{sat,298K}$ according to the
164 Clausius-Clapeyron relation:

$$165 C_{sat,T} = C_{sat,298K} \exp\left(\frac{\Delta H_{vap}}{R} \left(\frac{1}{298} - \frac{1}{T}\right)\right) \quad (1)$$

166 where T is the experimental temperature in K; ΔH_{vap} is the evaporation enthalpy in kJ mol^{-1} ,
167 which can be estimated based on $C_{sat,298K}$ by (Stark et al., 2017)

$$168 \Delta H_{vap} = -5.7 \times \log_{10} C_{sat,298K} + 129 \quad (2)$$

169 In the volatility basis set, we use the following volatility classes: ultra-low VOC (ULVOC,
170 $\log_{10} C_{sat} < -8.5$), extremely low VOC (ELVOC, $-8.5 < \log_{10} C_{sat} < -4.5$), low VOC (LVOC, $-4.5 < \log_{10} C_{sat} < -0.5$), semi VOC (SVOC, $-0.5 < \log_{10} C_{sat} < 2.5$), intermediate VOC (IVOC, $2.5 < \log_{10} C_{sat} < 6.5$), and VOC ($\log_{10} C_{sat} > 6.5$).



173 **2.4 Transport Model Simulations**

174 We coupled a 4-parameter 1D-VBS (10^0 , 10^1 , 10^2 , 10^3 $\mu\text{g m}^{-3}$) with the three-dimensional
175 chemical transport model (PMCAMx (Manavi and Pandis, 2022, 2024; Murphy and Pandis,
176 2009)) to implement our simulation chamber results. The PMCAMx model is briefly described
177 in Section S2 of the supplement. The stoichiometric yields of both isoprene and α -pinene are
178 temperature dependent based on the parameterization of Exp 1-5. Specifically: $T < 243$ K,
179 parameters based on Exp 1 (213 K); $243 \text{ K} \leq T < 273$ K, parameters from Exp 2 (243 K); 273
180 K $\leq T < 298$ K, parameters from Exp 3 (273 K); $298 \text{ K} \leq T < 313$ K, parameters from Exp 4
181 (298 K); $T \geq 313$ K, parameters from Exp 5 (313 K). Values for the Base and New cases are
182 provided in Table S1 and S2. The assumed dependence of the secondary organic aerosol mass
183 fraction on the organic aerosol mass concentration at different temperature ranges that is used
184 in the PMCAMx simulations is depicted in Figure S2.

185 The period considered in this model application is 5 June – 8 July 2012 (PEGASOS campaign)
186 in a European domain ($5400 \times 5832 \text{ km}^2$, Figure S3 and S4) with $36 \times 36 \text{ km}$ grid resolution,
187 and 14 vertical layers extending up to 7.5 km above ground. The temperature together with
188 other metrological parameters are provided by the Weather Research and Forecasting
189 meteorological model (WRF). Biogenic emissions are calculated by the MEGAN model
190 (Guenther et al., 2006), while anthropogenic and wildfire emissions are based on the GEMS
191 (Visschedijk et al., 2007) and IS4FIRES (Sofiev et al., 2008) inventories, respectively. In our
192 application, the domain average concentrations of isoprene and terpene in the simulated
193 European domain are 0.15 ppb and 0.04 ppb, respectively, with maximum predicted values of
194 2.8 ppb and 0.5 ppb. The spatial distributions of their average ground-level concentrations over
195 Europe are showed in Figure S3.

196 **3. Results**

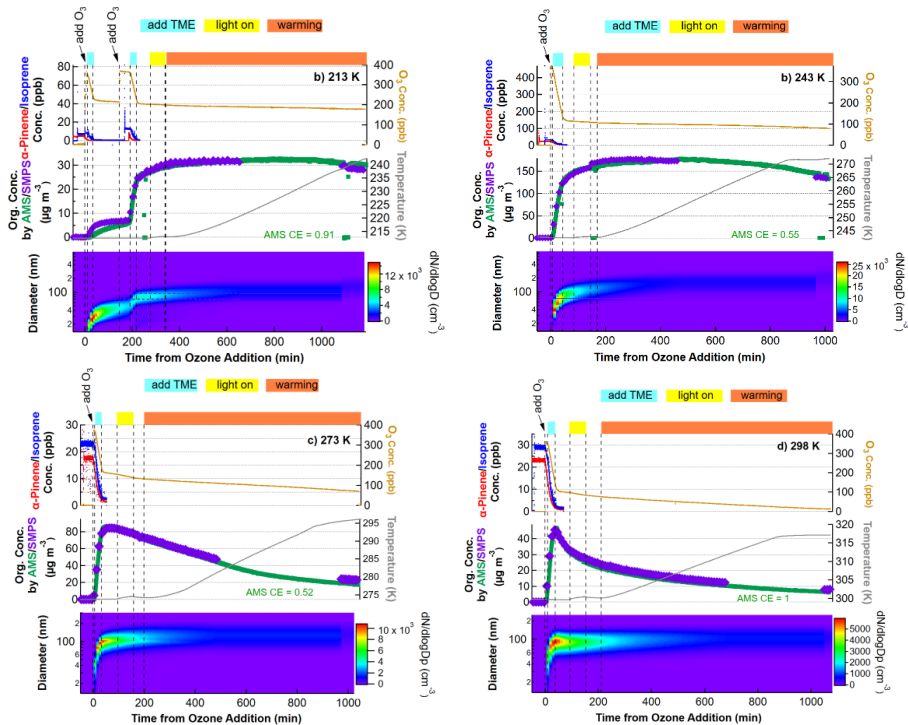
197 **3.1 Influence of temperature on particle-phase chemical composition**

198 In each experiment, the molecular composition of fresh SOA particles was characterized by
199 FIGAERO-iodide-CIMS using iodide as the reagent ion. The evolution of trace gases as well
200 as particle mass and size distribution for the oxidation of isoprene α -pinene mixture at all
201 temperatures are shown in Figure 1. We present first the identified cross dimers formed from
202 concurrent oxidation of isoprene and α -pinene (hereafter ‘ISO-AP dimers’) at 273 K. By
203 comparison of the particle-phase chemical composition among the experiment for sole α -pinene
204 (Exp 0), α -pinene and isoprene mixture at an equal concentration (Exp 3), and α -pinene and ^{13}C
205 labelled isoprene mixture at an equal concentration (Exp 6) shown in Table 1, we identified
206 ISO-AP dimers such as $\text{C}_{15}\text{H}_{20}\text{O}_{3.7}$, $\text{C}_{15}\text{H}_{22}\text{O}_{3.9}$, $\text{C}_{15}\text{H}_{24}\text{O}_{4.9}$, $\text{C}_{15}\text{H}_{26}\text{O}_{5.9}$, $\text{C}_{15}\text{H}_{28}\text{O}_{5.9}$, $\text{C}_{14}\text{H}_{20}\text{O}_{6.8}$,
207 $\text{C}_{14}\text{H}_{22}\text{O}_{5.9}$, and $\text{C}_{14}\text{H}_{24}\text{O}_{6.8}$. The identification of these cross dimers with 3-9 oxygen atoms
208 completes the list of highly oxygenated cross dimers with 9-13 oxygen atoms, which were
209 previously identified by a CIMS using nitrate as the reagent ion (McFiggans et al., 2019; Heinritzi
210 et al., 2020). Among all identified ISO-AP C_{14-15} cross dimers in Exp 3, $\text{C}_{15}\text{H}_{24}\text{O}_{4.9}$ and
211 $\text{C}_{14}\text{H}_{22}\text{O}_{5.9}$ contribute most to the total signals (21 %), followed by $\text{C}_{15}\text{H}_{26}\text{O}_{5.9}$, $\text{C}_{15}\text{H}_{28}\text{O}_{5.9}$, and
212 $\text{C}_{15}\text{H}_{22}\text{O}_{3.9}$ with signal fractions of 16 %, 11 %, and 11 %, respectively. The relative abundances
213 of these cross dimers in Exp 0 and Exp 6 are given in Figures S5-S6. Due to the scavenging of
214 OH and RO_2 radicals in the presence of isoprene, the relative contribution of solely α -pinene
215 derived C_{18-20} dimers from ozonolysis increases, while the contribution of dimers formed via



216 OH radical reactions decrease (Figure S7). This is qualitatively consistent with previous studies
217 (Mcfiggans et al., 2019; Heinritzi et al., 2020; Wang et al., 2021) performed at ~298 K.

218



219

220 Figure 1. Evolution of trace gases as well as particle mass and size for the oxidation of isoprene and α -
221 pinene mixtures at 213 K, 243 K, 273 K, and 298 K. The time axis is relative to the first addition of
222 ozone. The top shaded area of each plot shows the addition of TME to form OH radicals (blue), light on
223 (yellow), as well as warming period (orange).

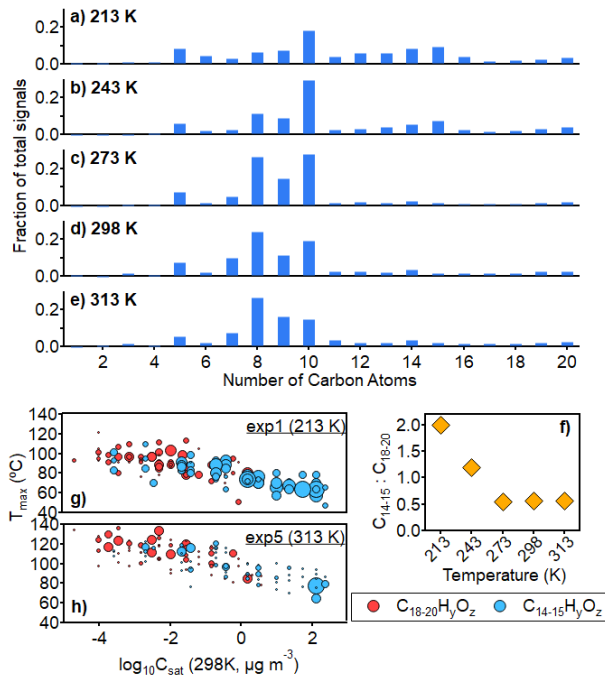
224 As shown in Figure 2, particle-phase C₁₄₋₁₅ ISO-AP cross dimers show higher signal fractions
225 at lower temperatures (in all detected compounds, 16% and 11% in total for 213 K and 243 K,
226 respectively) compared to those formed at higher temperatures (<4 % for 273 K, 298 K, and
227 313 K). For the dimers formed from α -pinene oxidation alone (C₁₈₋₂₀, hereafter ‘AP-AP
228 dimers’), including those from self- (i.e., both RO₂ involved in the dimerization originate either
229 from O₃ oxidation or from OH oxidation.) and cross-dimerization (i.e., between the two RO₂
230 radicals involved in the dimerization, one originates from O₃ oxidation, while the other
231 originates from OH oxidation) of RO₂ derived from α -pinene oxidation initiated by both O₃ and
232 OH radicals, lower temperatures exhibit slightly higher fractions with 8% - 9% at 213 – 243 K
233 compared to 4% - 6% at 273 – 313 K, consistent with previous observations (Zhang et al., 2015).
234 Most interestingly, the ratio of ISO-AP dimers to AP-AP dimers is 3.5 times higher at 213 K
235 (the ratio is 2) than that at 273 – 313 K (the ratios are 0.6, Figure 2f). This indicates that the
236 production of ISO-AP dimers plays a progressively more important role in SOA formation at
237 lower temperatures. Shown as Figure 2g and 1h, the higher ratio of ISO-AP dimers to AP-AP
238 dimers at 213 K than 313 K is mainly contributed by the greater formation of C₁₄₋₁₅ compounds.
239 The volatility (expressed by the saturation concentration at 298 K, C_{298K}^{*}) of ISO-AP dimers
240 (C_{298K}^{*} : 10^{-3.6}-10^{2.2} $\mu\text{g m}^{-3}$) is generally higher than that of AP-AP dimers (C_{298K}^{*} : 10^{-4.8}-10^{0.6}



241 $\mu\text{g m}^{-3}$), indicating that ISO-AP dimers are more volatile than AP-AP dimers when formed at
242 the same low temperatures. The difference in volatility between both groups of dimers is also
243 shown by their desorption temperature of maximum signal in the FIGAERO thermograms
244 (hereafter ' T_{\max} ') (Lopez-Hilfiker et al., 2014), which is an independent and qualitative
245 indicator of effective volatility compared to the volatility estimated by the parameterization
246 approach (Li et al., 2016) used in this work (Section S3). However, by comparing the particle
247 volatility distribution at different temperatures based on the gas- and particle-phase
248 measurement (i.e., $C^* = C_{OA} \frac{G_i}{P_i}$ (Gkatzelis et al., 2018)) at each temperature and based on the
249 Clausius-Clapeyron equation (Figure 3), the strong temperature dependence on the ISO-AP
250 dimers to AP-AP dimers between 213–273 K is suggested to be chemistry-driven. We interpret
251 this as follows. First, the gas-phase production rates of the two types of dimers may be
252 temperature dependent due to the temperature-affected concentrations of RO_2 radicals. The gas-
253 phase dimer formation rate via the bimolecular termination of $\text{RO}_2 + \text{R}'\text{O}_2 \rightarrow \text{ROOR}'$ rises
254 strongly with temperature (Quéléver et al., 2019). At lower temperatures, the lower rate
255 coefficient of α -pinene + O_3 (Khamaganov and Hites, 2001; Bernard et al., 2012) and higher
256 rate coefficient of isoprene + OH (Campuzano-Jost et al., 2000; Campuzano-Jost et al., 2004;
257 Dillon et al., 2017) lead to higher differential between the concentrations of C_{10}RO_2 from α -
258 pinene and C_5RO_2 from isoprene. Therefore, at lower temperatures, higher $[\text{C}_5\text{RO}_2]/[\text{C}_{10}\text{RO}_2]$
259 results in larger production of ISO-AP dimers compared with less formation of C_{20} AP-AP
260 dimers due to lower $[\text{C}_{10}\text{RO}_2]/[\text{C}_{10}\text{RO}_2]$. Besides, the other well-established dimer formation
261 pathway for α -pinene derived dimers, condensed-phase combination of acetyl peroxy radicals
262 yielding diacyl peroxides and their subsequent decomposition (Zhang et al., 2015) to produce
263 esters, carboxylic acids, and alcohols, is affected by temperature as well (Leffler and More,
264 1972; Lamb et al., 1965). Our observation suggests that the formation of ISO-AP dimers via
265 the diacyl peroxides pathway may be faster than that of AP-AP dimers at lower temperatures.
266 Second, previous studies (Trump and Donahue, 2014; Morino et al., 2020) have shown that the
267 decomposition rates of dimers depend on temperature and the type of dimers. Therefore, we
268 cannot exclude that AP-AP dimers decompose faster than ISO-AP dimers at lower temperature,
269 leading to higher condensed-phase ratios of $\text{C}_{14-15}/\text{C}_{18-20}$.

270 It should be noted that the sensitivity of iodide chemical ionization exhibits substantial
271 variability in detecting organic compounds with different functional groups. As a result, signal-
272 based analyses may not accurately represent the actual abundances of these species.
273 Nevertheless, comparing signal fractions across different experiments can provide valuable
274 insights into product distributions and underlying reaction mechanisms.

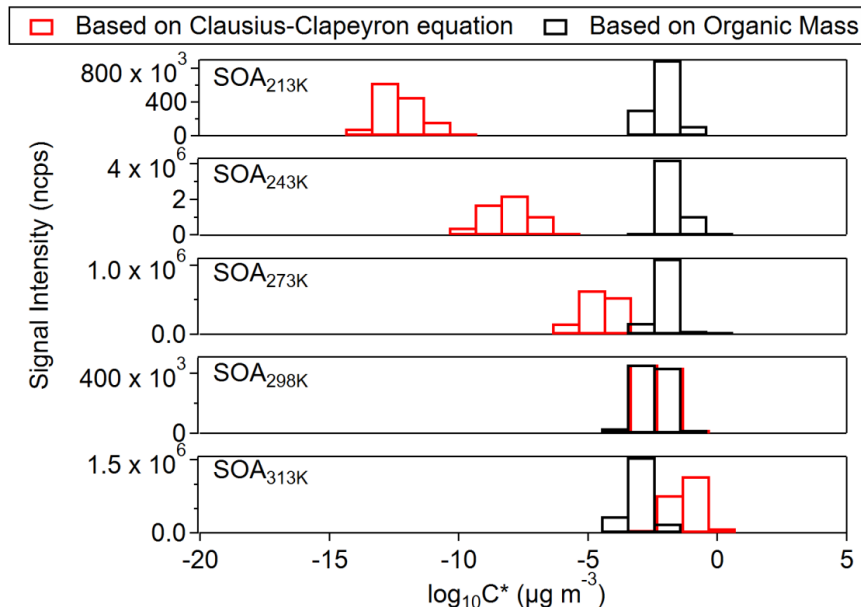
275 Overall, the nonmonotonic temperature dependence (Figure 2f) of the ratio of C_{14-15} to C_{18-20}
276 dimers between 213 – 313 K highlights the importance of the AP-AP dimer suppression by the
277 ISO-AP cross dimers. This is particularly relevant for biogenic particle formation and growth
278 in the real atmosphere especially at lower temperatures (Fu et al., 2009; Andreae et al., 2018).



279

280 Figure 2. Chemical composition of SOA derived from the mixture of isoprene and α -pinene at all temperatures
281 (Exp 1-5): 213 K (a), 243 K (b), 273 K (c), 298 K (d), and 313 K (e); the ratio of C_{14-15} compound signals to C_{18-20}
282 compound signals as a function of temperature (f); the distribution of C_{14-15} compounds and C_{18-20} compounds
283 with molecular T_{\max} corresponding to molecular logarithmic 298 K saturation concentration for Exp 1 at 213 K (g)
284 and Exp 5 at 313 K (h). Sizes of symbols in (g) and (h) correspond to the normalised signal abundance of molecules.

285



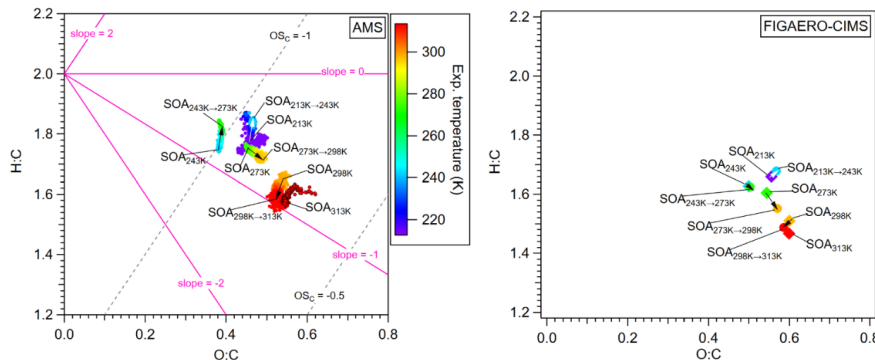
286

287 Figure 3. Volatility of _{C14-15} cross dimers formed at all temperatures calculated based on two
288 approaches: $C_{OA} \frac{g_i}{P_i}$ (Gkatzelis et al., 2018) and Clausius-Clapeyron equation.

289 **3.2 Influence of temperature on SOA aging**

290 To study the influence of temperature change on SOA formed at a specific temperature, we
291 warmed the fresh SOA particles up by 1.4-2.4 K/h over 10-12 hours, which resembles the
292 ambient temperature changing rate (~0.1-2 K/h) in the real atmosphere (Hansen et al., 2006).
293 The illumination has no significant effect on the bulk O:C, H:C and OSC (Figure S8). The
294 molecular chemical composition and volatility of fresh particles before warming are described
295 in the Supplementary Section S3. Most interestingly, by warming, SOA particles formed
296 initially at different temperatures showed distinct increments and/or decrements in bulk O:C
297 and H:C ratios as well as oxidation states (OSC) as measured by HR-AMS (Figure 4, Figure S9,
298 and Table S3). It indicates these SOA particles underwent distinct aging processes including
299 water uptake and evaporation when being warmed up.

300



301

302 Figure 4. Van-Krevelen diagram for SOA particles during the warming periods of Exp 1 (213 K to 243 K), Exp 2 (243 K to
 303 273 K), Exp 3 (273 K to 298 K), Exp 4 (298 K to 313 K), and Exp 5 (313 K) from HR-AMS measurements (left) and FIGAERO-
 304 iodide-CIMS measurements mean values (right, symbols of diamonds and circles for warming start and end, respectively).
 305 Arrows are for guiding from the start to end of the warming periods. Symbols are coloured by temperatures. The carbon
 306 oxidation state ($OS_c = 2 O:C - H:C$) is shown with a grey dashed line. The pink lines with different slopes represent various
 307 reaction pathways: slope = 2 (hydration); slope = 0 (formation of hydroxy/peroxy groups); slope = -1 (formation of carboxylic
 308 acids, or addition of both hydroxy and carbonyl groups); slope = -2 (addition of carbonyl groups).

309 We observed a clear increase of O:C ratios (from 0.36 to 0.54 from HR-AMS measurements,
 310 from 0.5 to 0.6 from FIGAERO-iodide-CIMS measurements) of fresh SOA particles formed
 311 between 243 K and 313 K (Figure 4). One exception is the particles formed at 213 K. The O:C
 312 ratio of the fresh SOA_{213K} (0.45 from HR-AMS measurement, 0.55 from FIGAERO-iodide-
 313 CIMS measurement) is higher than that of SOA_{243K}, contrary to the lower O:C ratios of particles
 314 formed at lower temperatures. This may result from the higher ratios of initial O₃ to VOCs
 315 concentrations (~19) in Exp 1 at 213K compared to other experiments (~7) (details in Method).

316 According to the HR-AMS measurements, the bulk O:C and H:C ratios of SOA particles
 317 formed at 243 K (SOA_{243K}) increases from 0.36 to 0.4 and from 1.69 to 1.82, respectively,
 318 during gradual warming to 273 K (SOA_{243K→273K}). Although the incremental O:C change is
 319 small, the online HR-AMS measurements showed a significant trend during the warming
 320 process (Figure 4). The slope (=3.25) in the Van-Krevelen diagram indicates hydration
 321 reactions during warming (Schilling Fahnestock et al., 2015; Heald et al., 2010).
 322 Correspondingly, the oxidation state (OS_c) of bulk SOA_{243K} decreases from -0.97 to -1.02 for
 323 SOA_{243K→273K} (Figure S9). According to the FIGAERO-iodide-CIMS measurements, 18 %
 324 fraction of the particle-phase C_xH_yO_z signals are lost during warming of SOA from 243 K
 325 (SOA_{243K}) to 273 K (SOA_{243K→273K}) (Figure 5d). The loss of oxygenated organic compounds
 326 mainly involves C₅, C₈₋₁₀, and C₁₄₋₁₅ compounds (Figure 5h), which are identified as monomeric
 327 products from sole isoprene and sole α -pinene, and their ISO-AP dimers, respectively. However,
 328 the loss of these oxygenated organic compounds leads to no significant change in the H:C ratio
 329 (from 1.63 to 1.62) and O:C ratio (from 0.50 to 0.50) of the particle-phase C_xH_yO_z measured
 330 by FIGAERO-iodide-CIMS. Therefore, the increase in bulk O:C and H:C ratios of SOA
 331 measured by HR-AMS indicates not only hydration reactions (Schilling Fahnestock et al., 2015;
 332 Heald et al., 2010) but also potential losses of more oxidized compounds with low H:C ratios.
 333 The bulk SOA aging towards higher H:C and O:C ratios during warming is likely due not only
 334 to sample evaporation but also to the change in the particle phase state.

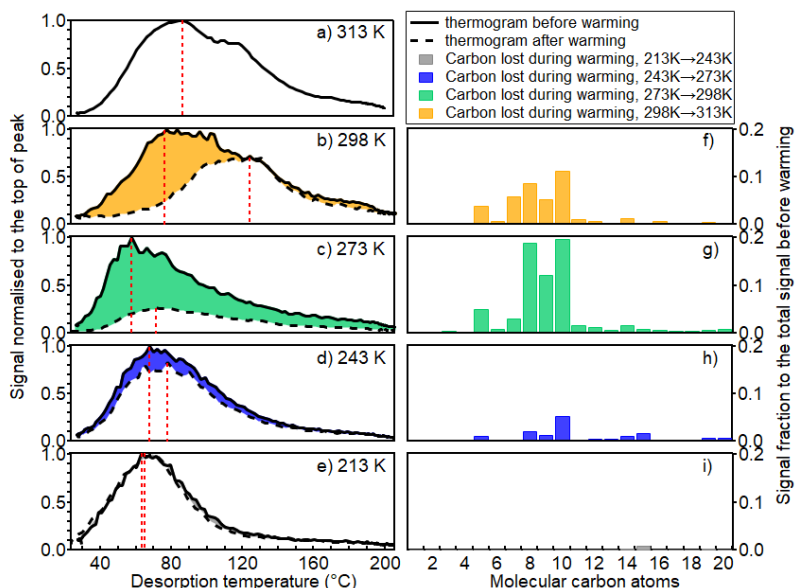


335 Similar changes of O:C and H:C ratios were observed for SOA_{213K} warmed to SOA_{213K→243K}.
336 Therefore, the SOA_{213K} warmed to SOA_{213K→243K} seems to undergo similar aging processes like
337 SOA_{243K} being warmed to SOA_{243K→273K}.

338 We characterized the viscosity of SOA particles by using the glass transition temperature, T_g
339 which is defined as the temperature at which an amorphous material transitions from a liquid-
340 like or semi-solid state to a glassy solid state. As the ambient temperature approaches or drops
341 below the T_g of a particle, its viscosity increases dramatically, often by several orders of
342 magnitude. Therefore, the phase state and viscosity of SOA can be inferred by characterizing
343 the T_g values. T_g was calculated for all detected organic compounds by FIGAERO-iodide-CIMS
344 using a parameterization approach (Derieux et al., 2018). In this study, SOA_{243K} is estimated to
345 be in a glassy solid state with a T_g of 289 K, comparable to the T_g values for sole isoprene- or
346 α -pinene-derived SOA reported in previous studies (Derieux et al., 2018; Ladino et al., 2014).
347 The high viscosity at low temperature kinetically inhibits the diffusion of water and large
348 organic molecules within the particle. Upon warming, the particle transitions from a glassy to
349 a semi-solid or liquid state, which facilitates the uptake and internal mixing of water. This
350 process can promote aqueous-phase reactions (e.g., hydrolysis, oxidation) that alter the organic
351 composition, increasing the H:C and O:C ratios. Therefore, water uptake and the potential
352 change of particle hygroscopicity (Shiraiwa et al., 2017; Pajunoja et al., 2015; Shiraiwa et al.,
353 2011) may contribute to increasing H:C and O:C ratios of bulk SOA_{243K} during warming from
354 243 K to 273 K.

355 In contrast, the bulk SOA_{273K} show a significant increase of OSc (from -0.87 to -0.75) and O:C
356 ratios (from 0.44 to 0.48) but a decrease of H:C ratios (from 1.76 to 1.73) during warming to
357 298 K (Figure 4). This tendency is consistent with the changes of O:C ratios and H:C ratios for
358 the oxygenated constituents measured by FIGAERO-iodide-CIMS. During warming of SOA_{273K}
359 to 298 K, 72.5 % of all particle-phase C_xH_yO_z compounds are lost, with OSc increasing from -
360 0.52 to -0.41, O:C from 0.54 to 0.57, and H:C ratios decreasing from 1.60 to 1.55. This indicates
361 that evaporation is the main loss process with higher losses of less oxidized compounds. This
362 is consistent with the analysis of HR-AMS spectra before and after warming (Figure S10) The
363 T_g we estimated for SOA_{273K} is 278 K, which is in between the temperatures of warming at the
364 start (273 K) and at the end (298 K). Therefore, the diffusion and evaporation of organic
365 molecules are gradually less hindered when particle phase state transits from solid/semi-solid
366 to liquid.

367 For the bulk SOA_{298K}, its estimated T_g is 283 K, which is evidently lower than the temperatures
368 during warming from 298 K to 313 K. This indicates that the SOA_{298K} remain in the liquid
369 phase during the whole warming process. As illustrated in Figure 4, warming of all SOA
370 compounds formed at 298 K leads to lower H:C (from 1.63 to 1.57) and O:C ratios (weekly
371 from 0.53 to 0.52), resulting in slightly higher OSc values (from -0.57 to -0.53). During
372 warming from 298 to 313 K, 40.2 % of all particle-phase C_xH_yO_z compounds were lost, by
373 substantial evaporation. However, the evaporation induces only small changes of O:C ratio
374 from 0.60 (SOA_{298K}) to 0.59 (SOA_{298K→313K}), H:C ratio from 1.51 to 1.49, and OSc from -0.31
375 to -0.32 for oxygenated organics, even though the trend is clear as shown in Figure 4. As the
376 reduction in H:C ratio is around 2 times higher than the reduction in O:C ratio for bulk SOA_{298K}
377 particles during the warming to 313 K, We infer that there might be water evaporation due to
378 the potential particle-phase dehydration reactions involving elimination of H₂O.



379

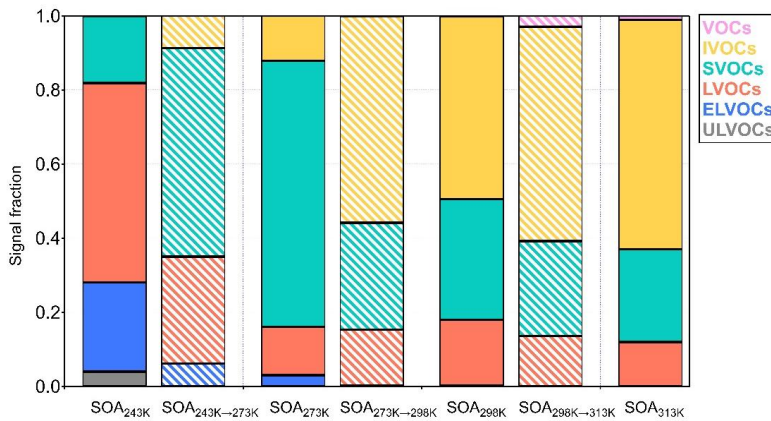
380 Figure 5. FIGAERO-iodide-CIMS thermograms of particles before and after warming process for all experiments
381 ((a) for 313 K, (b) for 298 K, (c) for 273 K, (d) for 243 K, and (e) for 213 K), and the corresponding carbon
382 distributions of molecules lost during warming (f-i). Black solid and dashed lines show the thermograms of
383 particles sampled before and after warming, respectively. The thermograms are normalized to the peak signals of
384 each thermogram before warming. Red vertical dashed lines indicate the T_{\max} .

385 As illustrated in Figure 5, before warming, volatility indicated by the T_{\max} of the fresh particles
386 showed a non-monotonic trend. This is similar with previous findings in the β -caryophyllene
387 system (Gao et al., 2023), which is due to favoured condensation or oligomerization reactions
388 at lower temperature and less production of low volatile HOMs which show larger fractions at
389 warmer temperatures. During warming, the volatility of the particles is influenced by changes
390 in their chemical composition as the gas-particle equilibrium is re-established through phase
391 partitioning. As the temperature increases, more volatile organic compounds evaporate from
392 the particle phase. Consequently, the particle composition becomes enriched in the remaining
393 lower-volatile organic species. This is corroborated by the higher T_{\max} values observed in the
394 thermograms: SOA_{243K-273K} (78 °C) compared to SOA_{243K} (68 °C), SOA_{273K-298K} (71 °C)
395 compared to SOA_{273K} (57 °C), and SOA_{298K-313K} (124°C) compared to SOA_{298K} (77 °C), as
396 illustrated in Figure 5b-d. The results indicate that the overall effect of warming on the SOA
397 particle volatility is governed by the initial temperature-dependent chemical composition and
398 the corresponding glass transition temperature.

399 Further support comes from the distribution of volatility groups estimated by the
400 parameterization approach (Li et al., 2016) based on measured numbers of molecular carbon,
401 hydrogen, and oxygen atoms. During warming, evaporation leads to compositional changes that
402 enrich the relatively lower-volatility compounds. Concurrently, rising temperatures shift the
403 entire VBS toward higher apparent volatility, following the Clausius-Clapeyron relation. For
404 instance, despite the evaporation of some volatile components during warming from 243 K to
405 273 K, the resulting SOA_{243K-273K} particles exhibit higher overall apparent volatility, containing
406 only 35% of LVOC/ELVOC/ULVOC (Figure S11 and Figure 6). Similarly, in the warming
407 experiment from 273 K to 298 K, the fraction of LVOC/ELVOC/ULVOC decreased slightly



408 from 16% to 15%, and from 18% to 14% in the case of $\text{SOA}_{298\text{K}\rightarrow313\text{K}}$ compared to $\text{SOA}_{298\text{K}}$.
409 These results underscore the significant role of ambient temperature on the apparent volatility
410 of SOA particles.



411
412 Figure 6. Signal fraction of volatility groups (ULVOC, ELVOC, LVOC, SLVOC, IVOC, and VOC) in the SOA
413 particles before (solid bars) and after (striped bars) warming process, respectively. Colors refer to the volatility
414 groups.

415 It should be noted that the FIGAERO-iodide-CIMS exhibits higher sensitivity toward moderate
416 oxygenated compounds (e.g., 2-9 oxygen atoms) (Riva et al., 2019), which may introduce bias
417 in the VBS. Nevertheless, comparisons of signal-weighted VBS distributions across different
418 experimental conditions remain indicative of the effects of temperature and warming on particle
419 volatility and the related chemical processes.”

420 Please note, that other condensed-phase chemical reactions may play a role during warming
421 process as well, e.g., dimers may decompose due to their chemical instability (Pospisilova et
422 al., 2020; Surdu et al., 2024), and the formation and condensation of molecules such as
423 peroxyhemiacetal and aldol has been found to be reversible and temperature-dependent.
424 However, it requires further studies to address this question systematically.

425 Furthermore, the oxidation states (OSc) of SOA particles after warming were lower than that
426 of the particles formed directly at these temperatures. As mentioned above, increasing
427 temperatures during warming facilitate the evaporation of more volatile compounds. This
428 results in the organic components remaining in the particles being generally less volatile and
429 higher oxidized corresponding to a higher oxidation state of bulk SOA as measured by the HR-
430 AMS.

431 However, it cannot compensate for the composition difference (e.g., due to autoxidation
432 (Bianchi et al., 2019)) between $\text{SOA}_{243\text{K}}$ and $\text{SOA}_{273\text{K}}$ caused by different reaction pathways
433 and product distributions at the different formation temperatures. For example, the saturation
434 concentrations of the same compounds in $\text{SOA}_{243\text{K}\rightarrow273\text{K}}$ and $\text{SOA}_{273\text{K}}$ systems are the same
435 because they are both at 273 K. We compared the molecular chemical composition of
436 $\text{SOA}_{243\text{K}\rightarrow273\text{K}}$ and $\text{SOA}_{273\text{K}}$ (Figure S12c and g). The C₁₁₋₂₀ products make up a higher signal
437 fraction in $\text{SOA}_{243\text{K}\rightarrow273\text{K}}$ (66%) compared to the corresponding compound groups in the
438 $\text{SOA}_{273\text{K}}$ (43%), and vice versa for C₄₋₁₀ products. Higher mean OSc values are found for
439 dimeric groups of C₁₃₋₁₅ as well as C₂₀, and other products of C₆ and C₁₆ in $\text{SOA}_{273\text{K}}$, leading to



440 higher OSC for bulk SOA particles. Thus, we emphasize that, besides promoting the
441 condensation of condensable components, lower temperatures chemically enhance the
442 formation of both ISO-AP cross dimers and AP-AP dimers, while higher temperatures may
443 favor the formation of higher oxidized products, e.g., via the autoxidation mechanism (Bianchi
444 et al., 2019).

445 For instance, $\text{SOA}_{298\text{K} \rightarrow 313\text{K}}$ has OSC values of -0.53 (HR-AMS) and -0.31 (FIGAERO-iodide-
446 CIMS), much lower than those of $\text{SOA}_{313\text{K}}$ (-0.49 by HR-AMS and -0.27 by FIGAERO-iodide-
447 CIMS). By comparing the molecular chemical composition of both particles at 313 K (Figure
448 S12 a and e), the higher mean OSC values for carbon groups of C_{4-10} in SOA formed directly at
449 313 K cause the increase of overall OSC of oxygenated products. This confirms again that higher
450 temperatures favour the formation of higher oxidized products.

451 In addition, C_{8-10} compounds (mean formula $\text{C}_{8.4}\text{H}_{12.4}\text{O}_{5.0}$) in $\text{SOA}_{298\text{K} \rightarrow 313\text{K}}$ have a T_{\max} of 100
452 °C. However, C_{8-10} compounds have a similar mean formula ($\text{C}_{8.5}\text{H}_{12.5}\text{O}_{5.3}$) in $\text{SOA}_{313\text{K}}$ but have
453 a lower T_{\max} of 82 °C. This implies that C_{8-10} compounds consist of varying monomeric isomers
454 with significantly different volatilities, being less volatile in $\text{SOA}_{298\text{K} \rightarrow 313\text{K}}$ and more volatile in
455 $\text{SOA}_{313\text{K}}$.

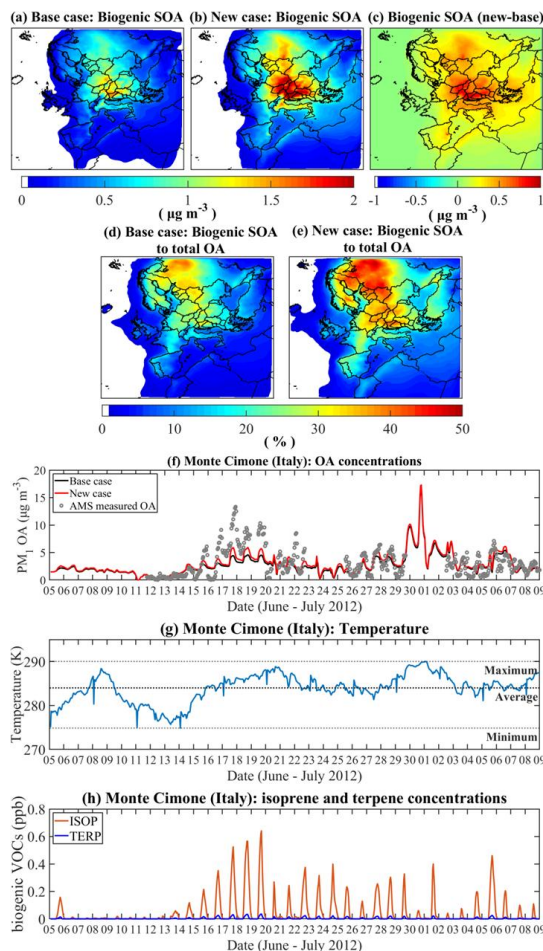
456 Besides, although $\text{SOA}_{273\text{K} \rightarrow 298\text{K}}$ has the largest OSC increment (-0.75 for bulk, -0.41 for
457 oxygenated constituents) from its initial particles before warming among all particles discussed,
458 its oxidation state is still significantly lower than $\text{SOA}_{298\text{K}}$ (-0.56 for bulk, -0.31 for oxygenated
459 constituents). This is consistent with the somewhat higher volatility of $\text{SOA}_{273\text{K} \rightarrow 298\text{K}}$ (T_{\max} of
460 71 °C) than $\text{SOA}_{298\text{K}}$ (T_{\max} of 77 °C, Figure 5b and c) observed. All compound groups remaining
461 after warming have higher mean OSC except for C_4 (Figure S12). This means that the
462 compounds in most compound groups are more oxidized when formed at 298 K. Thus, we
463 conclude that besides promoting the evaporation of particle-phase compounds, higher
464 temperatures also enhance the formation of higher oxidized products in SOA from oxidation of
465 α -pinene and isoprene mixtures.

466 **3.3 Modelling the impact of cross dimers for real world scenarios**

467 The relevance of these findings is corroborated by model simulations that incorporates the new
468 VBS parameterization derived below, including mixed dimers. The results discussed above are
469 based on experiments with equal initial amounts of α -pinene and isoprene. However, in the
470 natural atmosphere, the α -pinene to isoprene ratios can vary substantially for different
471 temperatures (seasons, day/night) and in different regions, e.g., boreal forest, tropical forest,
472 and temperate regions. The averaged ratio of isoprene to terpenes (including other monoterpene
473 compounds) over Europe during the simulation period is predicted to be 3.75 (Figure S3). With
474 α -pinene representing terpenes, simulations using the PMCAMx chemical transport model
475 (Tsimplidi et al., 2010; Fountoukis et al., 2011; Murphy and Pandis, 2009) show that when the
476 C_{14-15} ISO-AP dimers are considered under different temperatures, the predicted mass
477 concentration of organics over Europe is significantly enhanced. The mean ground-level PM_1
478 biogenic SOA mass concentrations over Europe for the simulated period are found to increase
479 by 47% from $0.23 \mu\text{g m}^{-3}$ with the original setup (Base case, Table S1) to $0.41 \mu\text{g m}^{-3}$ by
480 utilizing the new VBS parameterization including the temperature dependent C_{14-15} ISO-AP
481 cross dimers (New case, Table S2) (Figure 7a, b, c). The contribution of biogenic SOA to the
482 total OA mass increased from 9 to 14 % (Figure 7d, e). Specifically, in the New case, the
483 predicted ground-level OA mass concentrations are on average higher by $0.6 \mu\text{g m}^{-3}$ for four
484 measuring stations located in Italy (Figure S4), as shown in Figure S13.



485 During the simulated period, the isoprene emissions are greater over Croatia than other
 486 European areas. As a result, the difference in monthly averaged ground-level biogenic SOA
 487 concentrations between the two simulations is larger in Croatia ($0.9 \mu\text{g m}^{-3}$) than the domain
 488 average ($0.4 \mu\text{g m}^{-3}$). Figure S14 shows the correlation between isoprene concentrations and
 489 the enhancement of biogenic SOA mass predicted in the New case compared to the Base case
 490 over Croatia. In addition, due to the synergetic effect of relatively high concentrations of
 491 biogenic precursors and higher temperatures (Figure 7g-h), the simulated biogenic SOA
 492 concentrations at the site of Monte Cimone (2165 m.a.s.l.) show a better fit with the observed
 493 values compared to the Base case (Figure 7f).



494

495 Figure 7. The effect of the newly developed VBS parametrization on the predicted ground-level concentrations of
 496 biogenic SOA and total OA in PM_1 over Europe. Spatial distribution of the domain average biogenic SOA
 497 concentrations predicted utilizing (a) the original parametrization (Base case); (b) the new parameters derived
 498 considering the temperature dependent ISO-AP cross dimers (New case) and (c) the difference between the two
 499 simulations (New case – Base case); the contribution of the predicted biogenic SOA to the total OA concentrations
 500 over Europe in (d) the Base case and (e) the New case; (f) hourly ground-level OA concentrations predicted by the
 501 two simulations and measured by HR-AMS in the measuring site of Monte Cimone (Italy) during the PEGASUS
 502 campaign (June-July 2019); (g) the simulated hourly temperature profile (1st simulation layer) and (h) the predicted
 503 isoprene (ISOP) and terpene (TERP) ground-level concentrations over the measuring site for the simulated period.



504 **4. Conclusions**

505 This study utilized ^{13}C -labeled isoprene to identify cross-dimeric products from parallel
506 oxidation of isoprene and α -pinene while examining SOA composition and volatility covering
507 most tropospheric conditions with temperatures between 213 K and 313 K. The identified C_{14}
508 $_{15}$ ISO-AP cross dimers suppress the formation of the α -pinene self-dimers (AP-AP). This is
509 achieved by competing with α -pinene-derived peroxy radicals (which are generated via OH-
510 oxidation), thereby inhibiting their reactions. This suppression effect is more pronounced at
511 lower temperatures between 213 – 273 K, while it is not temperature-sensitive above 273 K.
512 SOA components observed are more oxidized at higher temperatures which is consistent with
513 previous studies, potentially driven by a larger contribution from autoxidation pathways (Gao
514 et al., 2022; Bianchi et al., 2019; Ye et al., 2019). Warming experiments reveal significant
515 volatility changes: SOA formed at 243 K is and remains solid/semi-solid, losing only 18% of
516 particle-phase compounds upon warming to 273 K. In contrast, SOA formed at 273 K
517 undergoes substantial transition from a semi-solid to a liquid phase when being warmed to 298
518 K, losing 72% of its mass. At 298 K, SOA shows lower O:C ratios and a 42% loss of oxygenated
519 organics when warmed to 313 K. SOA formed directly at higher temperatures is more oxidized
520 but more volatile than SOA formed at lower temperatures and subsequently warmed. This
521 observation has implications for SOA evolution over diurnal cycles. For example, in mid-
522 latitude or tropical environments, SOA formed during warmer daytime hours may be more
523 oxidized yet more volatile to reversible evaporation. In contrast, SOA generated during cooler
524 nighttime periods would be less oxidized but more persistent, forming a low-volatility reservoir.
525 This daily alternation could significantly influence the overall lifetime, chemical aging, and
526 mass yield of SOA particles on a regional scale.

527 Implementing this new mechanistic and volatility information in the PMCAMx model resulted
528 in higher predicted SOA over Europe. Future studies should extend this modelling to a broader
529 ground-level temperature range and evaluate it with extensive field data. Furthermore, although
530 this study focuses on isoprene and α -pinene mixtures, other biogenic and anthropogenic VOC
531 mixtures may exhibit similar temperature-sensitive behaviour. Therefore, further studies are
532 warranted to elucidate the impact of temperature on SOA formation from diverse VOC mixtures,
533 which will extend our understanding and improve predictions in the context of a warming
534 climate.

535 **Data availability**

536 Data used in this manuscript are publicly available (KITopen data link once DOI is available).

537 **Acknowledgements**

538 This work was supported by H2020 European Research Council (CHAPAs (grant no. 850614)).
539 L.G., and J.S. acknowledge the China Scholarship Council (CSC) for financial support and the
540 Graduate School for Climate and Environment (GRACE). The authors thank the IMK-AAF
541 technicians at the KIT for their support of this work.

542 **Author contributions**

543 L.G and H.S designed the study. Chamber experiments were carried out by L.G, H.S, and J.S.
544 Data analysis and interpretation were performed by L.G, J.S., H.S, C.M, and C.W. Model
545 simulations and interpretation were done by S.E.I.M, S.N.P, L.G, and H.S. The manuscript was



546 written by L.G, with input from S.E.I.M, C.M, J.S, C.W, T.L, S.N.P, and H.S. All co-authors
547 commented on the manuscript.

548 **Competing interests**

549 The authors declare no competing financial interest. Please note, that at least one of the authors
550 is co-editor of ACP.

551



552 **References**

553 Andreae, M. O., Afchine, A., Albrecht, R., Holanda, B. A., Artaxo, P., Barbosa, H. M. J., Borrmann, S.,
554 Cecchini, M. A., Costa, A., Dollner, M., Fütterer, D., Järvinen, E., Jurkat, T., Klimach, T., Konemann, T.,
555 Knoté, C., Krämer, M., Krisna, T., Machado, L. A. T., Mertes, S., Minikin, A., Pöhlker, C., Pöhlker, M. L.,
556 Pöschl, U., Rosenfeld, D., Sauer, D., Schlager, H., Schnaiter, M., Schneider, J., Schulz, C., Spanu, A.,
557 Sperling, V. B., Voigt, C., Walser, A., Wang, J., Weinzierl, B., Wendisch, M., and Ziereis, H.: Aerosol
558 characteristics and particle production in the upper troposphere over the Amazon Basin, *Atmos. Chem.
559 Phys.*, 18, 921-961, 10.5194/acp-18-921-2018, 2018.

560 Aubry, T. J., Staunton-Sykes, J., Marshall, L. R., Haywood, J., Abraham, N. L., and Schmidt, A.: Climate
561 change modulates the stratospheric volcanic sulfate aerosol lifecycle and radiative forcing from
562 tropical eruptions, *Nat. Commun.*, 12, 4708, 10.1038/s41467-021-24943-7, 2021.

563 Bernard, F., Fedioun, I., Peyroux, F., Quiggars, A., Daële, V., and Mellouki, A.: Thresholds of secondary
564 organic aerosol formation by ozonolysis of monoterpenes measured in a laminar flow aerosol reactor,
565 *J. Aerosol Sci.*, 43, 14-30, <https://doi.org/10.1016/j.jaerosci.2011.08.005>, 2012.

566 Bianchi, F., Kurtén, T., Riva, M., Mohr, C., Rissanen, M. P., Roldin, P., Berndt, T., Crounse, J. D.,
567 Wennberg, P. O., Mentel, T. F., Wildt, J., Junninen, H., Jokinen, T., Kulmala, M., Worsnop, D. R.,
568 Thornton, J. A., Donahue, N., Kjaergaard, H. G., and Ehn, M.: Highly Oxygenated Organic Molecules
569 (HOM) from Gas-Phase Autoxidation Involving Peroxy Radicals: A Key Contributor to Atmospheric
570 Aerosol, *Chemical Reviews*, 119, 3472-3509, 10.1021/acs.chemrev.8b00395, 2019.

571 Bilde, M., Barsanti, K., Booth, M., Cappa, C. D., Donahue, N. M., Emanuelsson, E. U., McFiggans, G.,
572 Krieger, U. K., Marcolli, C., Topping, D., Ziemann, P., Barley, M., Clegg, S., Dennis-Smither, B., Hallquist,
573 M., Hallquist, Å. M., Khlystov, A., Kulmala, M., Mogensen, D., Percival, C. J., Pope, F., Reid, J. P., Ribeiro
574 da Silva, M. A. V., Rosenoern, T., Salo, K., Soonsin, V. P., Yli-Juuti, T., Prisle, N. L., Pagels, J., Rarey, J.,
575 Zardini, A. A., and Riipinen, I.: Saturation Vapor Pressures and Transition Enthalpies of Low-Volatility
576 Organic Molecules of Atmospheric Relevance: From Dicarboxylic Acids to Complex Mixtures, *Chem.
577 Rev.*, 115, 4115-4156, 10.1021/cr5005502, 2015.

578 Campuzano-Jost, P., Williams, M. B., D'Otton, L., and Hynes, A. J.: Kinetics and Mechanism of the
579 Reaction of the Hydroxyl Radical with h8-Isoprene and d8-Isoprene: Isoprene Absorption Cross
580 Sections, Rate Coefficients, and the Mechanism of Hydroperoxyl Radical Production, *J. Phys. Chem. A*,
581 108, 1537-1551, 10.1021/jp0363601, 2004.

582 Campuzano-Jost, P., Williams, M. B., O'Ttome, L., and Hynes, A. J.: Kinetics of the OH-initiated
583 oxidation of isoprene, *Geophys. Res. Lett.*, 27, 693-696, <https://doi.org/10.1029/1999GL010995>, 2000.

584 Carlton, A. G., Wiedinmyer, C., and Kroll, J. H.: A review of Secondary Organic Aerosol (SOA) formation
585 from isoprene, *Atmos. Chem. Phys.*, 9, 4987-5005, 10.5194/acp-9-4987-2009, 2009.

586 Curtius, J., Heinritzi, M., Beck, L. J., Pöhlker, M. L., Tripathi, N., Krumm, B. E., Holzbeck, P., Nussbaumer,
587 C. M., Hernández Pardo, L., Klimach, T., Barmpounis, K., Andersen, S. T., Bardakov, R., Bohn, B., Cecchini,
588 M. A., Chaboureau, J.-P., Dauhut, T., Dienhart, D., Dörich, R., Edtbauer, A., Giez, A., Hartmann, A.,
589 Holanda, B. A., Joppe, P., Kaiser, K., Keber, T., Klebach, H., Krüger, O. O., Kürten, A., Mallaun, C., Marno,
590 D., Martinez, M., Monteiro, C., Nelson, C., Ort, L., Raj, S. S., Richter, S., Ringsdorf, A., Rocha, F., Simon,
591 M., Sreekumar, S., Tsokankunku, A., Unfer, G. R., Valenti, I. D., Wang, N., Zahn, A., Zauner-Wieczorek,
592 M., Albrecht, R. I., Andreae, M. O., Artaxo, P., Crowley, J. N., Fischer, H., Harder, H., Herdies, D. L.,
593 Machado, L. A. T., Pöhlker, C., Pöschl, U., Possner, A., Pozzer, A., Schneider, J., Williams, J., and Lelieveld,
594 J.: Isoprene nitrates drive new particle formation in Amazon's upper troposphere, *Nature*, 636, 124-
595 130, 10.1038/s41586-024-08192-4, 2024.

596 DeRieux, W. S. W., Li, Y., Lin, P., Laskin, J., Laskin, A., Bertram, A. K., Nizkorodov, S. A., and Shiraiwa, M.:
597 Predicting the glass transition temperature and viscosity of secondary organic material using molecular
598 composition, *Atmos. Chem. Phys.*, 18, 6331-6351, 10.5194/acp-18-6331-2018, 2018.

599 Dillon, T. J., Dulitz, K., Groß, C. B. M., and Crowley, J. N.: Temperature-dependent rate coefficients for
600 the reactions of the hydroxyl radical with the atmospheric biogenics isoprene, alpha-pinene and delta-
601 3-carene, *Atmos. Chem. Phys.*, 17, 15137-15150, 10.5194/acp-17-15137-2017, 2017.



602 Donahue, N. M., Robinson, A. L., Stanier, C. O., and Pandis, S. N.: Coupled Partitioning, Dilution, and
603 Chemical Aging of Semivolatile Organics, *Environ. Sci. Technol.*, 40, 2635-2643, 10.1021/es052297c,
604 2006.

605 Fountoukis, C., Racherla, P. N., Denier van der Gon, H. A. C., Polymeneas, P., Charalampidis, P. E., Pilinis,
606 C., Wiedensohler, A., Dall'Osto, M., O'Dowd, C., and Pandis, S. N.: Evaluation of a three-dimensional
607 chemical transport model (PMCAMx) in the European domain during the EUCAARI May 2008 campaign,
608 *Atmos. Chem. Phys.*, 11, 10331-10347, 10.5194/acp-11-10331-2011, 2011.

609 Fu, P., Kawamura, K., Chen, J., and Barrie, L. A.: Isoprene, Monoterpene, and Sesquiterpene Oxidation
610 Products in the High Arctic Aerosols during Late Winter to Early Summer, *Environ. Sci. Technol.*, 43,
611 4022-4028, 10.1021/es803669a, 2009.

612 Gao, L., Song, J., Mohr, C., Huang, W., Vallon, M., Jiang, F., Leisner, T., and Saathoff, H.: Kinetics, SOA
613 yields, and chemical composition of secondary organic aerosol from β -caryophyllene ozonolysis with
614 and without nitrogen oxides between 213 and 313 K , *Atmos. Chem. Phys.*, 22, 6001-6020,
615 10.5194/acp-22-6001-2022, 2022.

616 Gao, L., Buchholz, A., Li, Z., Song, J., Vallon, M., Jiang, F., Möhler, O., Leisner, T., and Saathoff, H.:
617 Volatility of Secondary Organic Aerosol from β -Caryophyllene Ozonolysis over a Wide Tropospheric
618 Temperature Range, *Environmental Science & Technology*, 57, 8965-8974, 10.1021/acs.est.3c01151,
619 2023.

620 Gkatzelis, G. I., Hohaus, T., Tillmann, R., Gensch, I., Müller, M., Eichler, P., Xu, K. M., Schlag, P., Schmitt,
621 S. H., Yu, Z., Wegener, R., Kaminski, M., Holzinger, R., Wisthaler, A., and Kiendler-Scharr, A.: Gas-to-
622 particle partitioning of major biogenic oxidation products: a study on freshly formed and aged biogenic
623 SOA, *Atmos. Chem. Phys.*, 18, 12969-12989, 10.5194/acp-18-12969-2018, 2018.

624 Guenther, A., Karl, T., Harley, P., Wiedinmyer, C., Palmer, P. I., and Geron, C.: Estimates of global
625 terrestrial isoprene emissions using MEGAN (Model of Emissions of Gases and Aerosols from Nature),
626 *Atmos. Chem. Phys.*, 6, 3181-3210, 10.5194/acp-6-3181-2006, 2006.

627 Hallquist, M., Wenger, J. C., Baltensperger, U., Rudich, Y., Simpson, D., Claeys, M., Dommen, J.,
628 Donahue, N. M., George, C., Goldstein, A. H., Hamilton, J. F., Herrmann, H., Hoffmann, T., Iinuma, Y.,
629 Jang, M., Jenkin, M. E., Jimenez, J. L., Kiendler-Scharr, A., Maenhaut, W., McFiggans, G., Mentel, T. F.,
630 Monod, A., Prévôt, A. S. H., Seinfeld, J. H., Surratt, J. D., Szmigielski, R., and Wildt, J.: The formation,
631 properties and impact of secondary organic aerosol: current and emerging issues, *Atmos. Chem. Phys.*,
632 9, 5155-5236, 10.5194/acp-9-5155-2009, 2009.

633 Hansen, J., Sato, M., Ruedy, R., Lo, K., Lea, D. W., and Medina-Elizade, M.: Global temperature change,
634 *Proc. Natl. Acad. Sci.*, 103, 14288-14293, doi:10.1073/pnas.0606291103, 2006.

635 Heald, C. L., Kroll, J. H., Jimenez, J. L., Docherty, K. S., DeCarlo, P. F., Aiken, A. C., Chen, Q., Martin, S. T.,
636 Farmer, D. K., and Artaxo, P.: A simplified description of the evolution of organic aerosol composition
637 in the atmosphere, *Geophysical Research Letters*, 37, <https://doi.org/10.1029/2010GL042737>, 2010.

638 Heinritzi, M., Dada, L., Simon, M., Stolzenburg, D., Wagner, A. C., Fischer, L., Ahonen, L. R., Amanatidis,
639 S., Baalbaki, R., Baccarini, A., Bauer, P. S., Baumgartner, B., Bianchi, F., Brilke, S., Chen, D., Chiu, R., Dias,
640 A., Dommen, J., Duplissy, J., Finkenzeller, H., Frege, C., Fuchs, C., Garmash, O., Gordon, H., Granzin, M.,
641 El Haddad, I., He, X., Helm, J., Hofbauer, V., Hoyle, C. R., Kangasluoma, J., Keber, T., Kim, C., Kürten, A.,
642 Lamkaddam, H., Laurila, T. M., Lampilahti, J., Lee, C. P., Lehtipalo, K., Leiminger, M., Mai, H.,
643 Makhmutov, V., Manninen, H. E., Marten, R., Mathot, S., Mauldin, R. L., Mentler, B., Molteni, U., Müller,
644 T., Nie, W., Nieminen, T., Onnela, A., Partoll, E., Passananti, M., Petäjä, T., Pfeifer, J., Pospisilova, V.,
645 Quéléver, L. L. J., Rissanen, M. P., Rose, C., Schobesberger, S., Scholz, W., Scholze, K., Sipilä, M., Steiner,
646 G., Stozhkov, Y., Tauber, C., Tham, Y. J., Vazquez-Pufleau, M., Virtanen, A., Vogel, A. L., Volkamer, R.,
647 Wagner, R., Wang, M., Weitz, L., Wimmer, D., Xiao, M., Yan, C., Ye, P., Zha, Q., Zhou, X., Amorim, A.,
648 Baltensperger, U., Hansel, A., Kulmala, M., Tomé, A., Winkler, P. M., Worsnop, D. R., Donahue, N. M.,
649 Kirkby, J., and Curtius, J.: Molecular understanding of the suppression of new-particle formation by
650 isoprene, *Atmos. Chem. Phys.*, 20, 11809-11821, 10.5194/acp-20-11809-2020, 2020.

651 Jimenez, J. L., Canagaratna, M. R., Donahue, N. M., Prevot, A. S. H., Zhang, Q., Kroll, J. H., DeCarlo, P.
652 F., Allan, J. D., Coe, H., Ng, N. L., Aiken, A. C., Docherty, K. S., Ulbrich, I. M., Grieshop, A. P., Robinson,



653 A. L., Duplissy, J., Smith, J. D., Wilson, K. R., Lanz, V. A., Hueglin, C., Sun, Y. L., Tian, J., Laaksonen, A.,
654 Raatikainen, T., Rautiainen, J., Vaattovaara, P., Ehn, M., Kulmala, M., Tomlinson, J. M., Collins, D. R.,
655 Cubison, M. J., E., Dunlea, J., Huffman, J. A., Onasch, T. B., Alfarra, M. R., Williams, P. I., Bower, K.,
656 Kondo, Y., Schneider, J., Drewnick, F., Borrmann, S., Weimer, S., Demerjian, K., Salcedo, D., Cottrell, L.,
657 Griffin, R., Takami, A., Miyoshi, T., Hatakeyama, S., Shimono, A., Sun, J. Y., Zhang, Y. M., Dzepina, K.,
658 Kimmel, J. R., Sueper, D., Jayne, J. T., Herndon, S. C., Trimborn, A. M., Williams, L. R., Wood, E. C.,
659 Middlebrook, A. M., Kolb, C. E., Baltensperger, U., and Worsnop, D. R.: Evolution of Organic Aerosols
660 in the Atmosphere, *Science*, 326, 1525-1529, doi:10.1126/science.1180353, 2009.
661 Jonsson, Å. M., Hallquist, M., and Ljungström, E.: The effect of temperature and water on secondary
662 organic aerosol formation from ozonolysis of limonene, Δ ;3-carene and α -pinene,
663 *Atmos. Chem. Phys.*, 8, 6541-6549, 10.5194/acp-8-6541-2008, 2008.
664 Kanakidou, M., Seinfeld, J. H., Pandis, S. N., Barnes, I., Dentener, F. J., Facchini, M. C., Van Dingenen,
665 R., Ervens, B., Nenes, A., Nielsen, C. J., Swietlicki, E., Putaud, J. P., Balkanski, Y., Fuzzi, S., Horth, J.,
666 Moortgat, G. K., Winterhalter, R., Myhre, C. E. L., Tsigaridis, K., Vignati, E., Stephanou, E. G., and Wilson,
667 J.: Organic aerosol and global climate modelling: a review, *Atmos. Chem. Phys.*, 5, 1053-1123,
668 10.5194/acp-5-1053-2005, 2005.
669 Khamaganov, V. G. and Hites, R. A.: Rate Constants for the Gas-Phase Reactions of Ozone with Isoprene,
670 α - and β -Pinene, and Limonene as a Function of Temperature, *J. Phys. Chem. A*, 105, 815-822,
671 10.1021/jp002730z, 2001.
672 Kiendler-Scharr, A., Wildt, J., Maso, M. D., Hohaus, T., Kleist, E., Mentel, T. F., Tillmann, R., Uerlings, R.,
673 Schurr, U., and Wahner, A.: New particle formation in forests inhibited by isoprene emissions, *Nature*,
674 461, 381-384, 10.1038/nature08292, 2009.
675 Kourtchev, I., Doussin, J. F., Giorio, C., Mahon, B., Wilson, E. M., Maurin, N., Pangui, E., Venables, D. S.,
676 Wenger, J. C., and Kalberer, M.: Molecular composition of fresh and aged secondary organic aerosol
677 from a mixture of biogenic volatile compounds: a high-resolution mass spectrometry study, *Atmos.*
678 *Chem. Phys.*, 15, 5683-5695, 10.5194/acp-15-5683-2015, 2015.
679 Kroll, J. H. and Seinfeld, J. H.: Chemistry of secondary organic aerosol: Formation and evolution of low-
680 volatility organics in the atmosphere, *Atmos. Environ.*, 42, 3593-3624,
681 <https://doi.org/10.1016/j.atmosenv.2008.01.003>, 2008.
682 Ladino, L. A., Zhou, S., Yakobi-Hancock, J. D., Aljawhary, D., and Abbatt, J. P. D.: Factors controlling the
683 ice nucleating abilities of α -pinene SOA particles, *J. Geophys. Res.*, 119, 9041-9051,
684 <https://doi.org/10.1002/2014JD021578>, 2014.
685 Lamb, R. C., Pacifici, J. G., and Ayers, P. W.: Organic Peroxides. IV. Kinetics and Products of
686 Decompositions of Cyclohexaneformyl and Isobutyryl Peroxides. BDPA as a Free-Radical Scavenger1, J.
687 *Am. Chem. Soc.*, 87, 3928-3935, 10.1021/ja01095a024, 1965.
688 Lamkaddam, H., Dommen, J., Ranjithkumar, A., Gordon, H., Wehrle, G., Krechmer, J., Majluf, F.,
689 Saliyanov, D., Schmale, J., Bjelić, S., Carslaw, K. S., El Haddad, I., and Baltensperger, U.: Large
690 contribution to secondary organic aerosol from isoprene cloud chemistry, *Sci. Adv.*, 7, eabe2952,
691 doi:10.1126/sciadv.abe2952, 2021.
692 Lee, B. H., Lopez-Hilfiker, F. D., Mohr, C., Kurtén, T., Worsnop, D. R., and Thornton, J. A.: An Iodide-
693 Adduct High-Resolution Time-of-Flight Chemical-Ionization Mass Spectrometer: Application to
694 Atmospheric Inorganic and Organic Compounds, *Environmental Science & Technology*, 48, 6309-6317,
695 10.1021/es500362a, 2014.
696 Leffler, J. E. and More, A. A.: Decomposition of bicyclo[2.2.2]-1-formyl and pivaloyl peroxides, *J. Am.*
697 *Chem. Soc.*, 94, 2483-2487, 10.1021/ja00762a048, 1972.
698 Li, H., Canagaratna, M. R., Riva, M., Rantala, P., Zhang, Y., Thomas, S., Heikkinen, L., Flaud, P. M.,
699 Villenave, E., Perraudeau, E., Worsnop, D., Kulmala, M., Ehn, M., and Bianchi, F.: Atmospheric organic
700 vapors in two European pine forests measured by a Vocus PTR-TOF: insights into monoterpane and
701 sesquiterpene oxidation processes, *Atmos. Chem. Phys.*, 21, 4123-4147, 10.5194/acp-21-4123-2021,
702 2021.



703 Li, Y., Pöschl, U., and Shiraiwa, M.: Molecular corridors and parameterizations of volatility in the
704 chemical evolution of organic aerosols, *Atmos. Chem. Phys.*, 16, 3327-3344, 10.5194/acp-16-3327-
705 2016, 2016.

706 Liu, Y., Su, H., Wang, S., Wei, C., Tao, W., Pöhlker, M. L., Pöhlker, C., Holanda, B. A., Krüger, O. O.,
707 Hoffmann, T., Wendisch, M., Artaxo, P., Pöschl, U., Andreae, M. O., and Cheng, Y.: Strong particle
708 production and condensational growth in the upper troposphere sustained by biogenic VOCs from the
709 canopy of the Amazon Basin, *Atmos. Chem. Phys.*, 23, 251-272, 10.5194/acp-23-251-2023, 2023.

710 Lopez-Hilfiker, F. D., Iyer, S., Mohr, C., Lee, B. H., D'Ambro, E. L., Kurtén, T., and Thornton, J. A.:
711 Constraining the sensitivity of iodide adduct chemical ionization mass spectrometry to multifunctional
712 organic molecules using the collision limit and thermodynamic stability of iodide ion adducts, *Atmos.*
713 *Meas. Tech.*, 9, 1505-1512, 10.5194/amt-9-1505-2016, 2016.

714 Lopez-Hilfiker, F. D., Mohr, C., Ehn, M., Rubach, F., Kleist, E., Wildt, J., Mentel, T. F., Lutz, A., Hallquist,
715 M., Worsnop, D., and Thornton, J. A.: A novel method for online analysis of gas and particle
716 composition: description and evaluation of a Filter Inlet for Gases and AEROsols (FIGAERO), *Atmos.*
717 *Meas. Tech.*, 7, 983-1001, 10.5194/amt-7-983-2014, 2014.

718 Lopez-Hilfiker, F. D., Mohr, C., Ehn, M., Rubach, F., Kleist, E., Wildt, J., Mentel, T. F., Carrasquillo, A. J.,
719 Daumit, K. E., Hunter, J. F., Kroll, J. H., Worsnop, D. R., and Thornton, J. A.: Phase partitioning and
720 volatility of secondary organic aerosol components formed from α -pinene ozonolysis and OH oxidation:
721 the importance of accretion products and other low volatility compounds, *Atmos. Chem. Phys.*, 15,
722 7765-7776, 10.5194/acp-15-7765-2015, 2015.

723 Mahowald, N.: Aerosol Indirect Effect on Biogeochemical Cycles and Climate, *Science*, 334, 794-796,
724 doi:10.1126/science.1207374, 2011.

725 Manavi, S. E. I. and Pandis, S. N.: A lumped species approach for the simulation of secondary organic
726 aerosol production from intermediate-volatility organic compounds (IVOCs): application to road
727 transport in PMCAMx-iv (v1.0), *Geosci. Model Dev.*, 15, 7731-7749, 10.5194/gmd-15-7731-2022, 2022.

728 Manavi, S. E. I. and Pandis, S. N.: Contribution of intermediate-volatility organic compounds from on-
729 road transport to secondary organic aerosol levels in Europe, *Atmos. Chem. Phys.*, 24, 891-909,
730 10.5194/acp-24-891-2024, 2024.

731 McFiggans, G., Mentel, T. F., Wildt, J., Pullinen, I., Kang, S., Kleist, E., Schmitt, S., Springer, M., Tillmann,
732 R., Wu, C., Zhao, D., Hallquist, M., Faxon, C., Le Breton, M., Hallquist, Å. M., Simpson, D., Bergström,
733 R., Jenkin, M. E., Ehn, M., Thornton, J. A., Alfarra, M. R., Bannan, T. J., Percival, C. J., Priestley, M.,
734 Topping, D., and Kiendler-Scharr, A.: Secondary organic aerosol reduced by mixture of atmospheric
735 vapours, *Nature*, 565, 587-593, 10.1038/s41586-018-0871-y, 2019.

736 Möhler, O., Stetzer, O., Schaefers, S., Linke, C., Schnaiter, M., Tiede, R., Saathoff, H., Krämer, M.,
737 Mangold, A., Budz, P., Zink, P., Schreiner, J., Mauersberger, K., Haag, W., Kärcher, B., and Schurath, U.:
738 Experimental investigation of homogeneous freezing of sulphuric acid particles in the aerosol chamber
739 AIDA, *Atmos. Chem. Phys.*, 3, 211-223, 10.5194/acp-3-211-2003, 2003.

740 Morino, Y., Sato, K., Jathar, S. H., Tanabe, K., Inomata, S., Fujitani, Y., Ramasamy, S., and Cappa, C. D.:
741 Modeling the Effects of Dimerization and Bulk Diffusion on the Evaporative Behavior of Secondary
742 Organic Aerosol Formed from α -Pinene and 1,3,5-Trimethylbenzene, *ACS Earth Space Chem.*, 4, 1931-
743 1946, 10.1021/acsearthspacechem.0c00106, 2020.

744 Murphy, B. N. and Pandis, S. N.: Simulating the Formation of Semivolatile Primary and Secondary
745 Organic Aerosol in a Regional Chemical Transport Model, *Environmental Science & Technology*, 43,
746 4722-4728, 10.1021/es803168a, 2009.

747 Owen, S. M., MacKenzie, A. R., Stewart, H., Donovan, R., and Hewitt, C. N.: BIOGENIC VOLATILE
748 ORGANIC COMPOUND (VOC) EMISSION ESTIMATES FROM AN URBAN TREE CANOPY, *Ecol. Appl.*, 13,
749 927-938, <https://doi.org/10.1890/01-5177>, 2003.

750 Paasonen, P., Asmi, A., Petäjä, T., Kajos, M. K., Äijälä, M., Junninen, H., Holst, T., Abbatt, J. P. D., Arneth,
751 A., Birmili, W., van der Gon, H. D., Hamed, A., Hoffer, A., Laakso, L., Laaksonen, A., Richard Leaitch, W.,
752 Plass-Dülmer, C., Pryor, S. C., Räisänen, P., Swietlicki, E., Wiedensohler, A., Worsnop, D. R., Kerminen,



753 V.-M., and Kulmala, M.: Warming-induced increase in aerosol number concentration likely to
754 moderate climate change, *Nat. Geosci.*, 6, 438-442, 10.1038/ngeo1800, 2013.

755 Pajunoja, A., Lambe, A. T., Hakala, J., Rastak, N., Cummings, M. J., Brogan, J. F., Hao, L., Paramonov, M.,
756 Hong, J., Prisle, N. L., Malila, J., Romakkaniemi, S., Lehtinen, K. E. J., Laaksonen, A., Kulmala, M., Massoli,
757 P., Onasch, T. B., Donahue, N. M., Riipinen, I., Davidovits, P., Worsnop, D. R., Petäjä, T., and Virtanen,
758 A.: Adsorptive uptake of water by semisolid secondary organic aerosols, *Geophys. Res. Lett.*, 42, 3063-
759 3068, <https://doi.org/10.1002/2015GL063142>, 2015.

760 Petersen, R., Holst, T., Mölder, M., Kljun, N., and Rinne, J.: Vertical distribution of sources and sinks of
761 volatile organic compounds within a boreal forest canopy, *Atmos. Chem. Phys.*, 23, 7839-7858,
762 10.5194/acp-23-7839-2023, 2023.

763 Pospisilova, V., Lopez-Hilfiker, F. D., Bell, D. M., El Haddad, I., Mohr, C., Huang, W., Heikkinen, L., Xiao,
764 M., Dommen, J., Prevot, A. S. H., Baltensperger, U., and Slowik, J. G.: On the fate of oxygenated organic
765 molecules in atmospheric aerosol particles, *Science Advances*, 6, eaax8922,
766 doi:10.1126/sciadv.aax8922, 2020.

767 Quéléver, L. L. J., Kristensen, K., Normann Jensen, L., Rosati, B., Teiwes, R., Daellenbach, K. R., Peräkylä,
768 O., Roldin, P., Bossi, R., Pedersen, H. B., Glasius, M., Bilde, M., and Ehn, M.: Effect of temperature on
769 the formation of highly oxygenated organic molecules (HOMs) from α -pinene ozonolysis, *Atmos. Chem.*
770 *Phys.*, 19, 7609-7625, 10.5194/acp-19-7609-2019, 2019.

771 Riva, M., Rantala, P., Krechmer, J. E., Peräkylä, O., Zhang, Y., Heikkinen, L., Garmash, O., Yan, C., Kulmala,
772 M., Worsnop, D., and Ehn, M.: Evaluating the performance of five different chemical ionization
773 techniques for detecting gaseous oxygenated organic species, *Atmos. Meas. Tech.*, 12, 2403-2421,
774 10.5194/amt-12-2403-2019, 2019.

775 Saathoff, H., Naumann, K. H., Möhler, O., Jonsson, Å. M., Hallquist, M., Kiendler-Scharr, A., Mentel, T.
776 F., Tillmann, R., and Schurath, U.: Temperature dependence of yields of secondary organic aerosols
777 from the ozonolysis of α -pinene and limonene, *Atmos. Chem. Phys.*, 9, 1551-1577, 10.5194/acp-9-
778 1551-2009, 2009.

779 Schilling Fahnestock, K. A., Yee, L. D., Loza, C. L., Coggon, M. M., Schwantes, R., Zhang, X., Dalleska, N.
780 F., and Seinfeld, J. H.: Secondary Organic Aerosol Composition from C12 Alkanes, *The Journal of*
781 *Physical Chemistry A*, 119, 4281-4297, 10.1021/jp501779w, 2015.

782 Schulz, C., Schneider, J., Amorim Holanda, B., Appel, O., Costa, A., de Sá, S. S., Dreiling, V., Fütterer, D.,
783 Jurkat-Witschas, T., Klimach, T., Knote, C., Krämer, M., Martin, S. T., Mertes, S., Pöhlker, M. L., Sauer,
784 D., Voigt, C., Walser, A., Weinzierl, B., Ziereis, H., Zöger, M., Andreae, M. O., Artaxo, P., Machado, L. A.
785 T., Pöschl, U., Wendisch, M., and Borrmann, S.: Aircraft-based observations of isoprene-epoxydiol-
786 derived secondary organic aerosol (IEPOX-SOA) in the tropical upper troposphere over the Amazon
787 region, *Atmos. Chem. Phys.*, 18, 14979-15001, 10.5194/acp-18-14979-2018, 2018.

788 Sheehan, P. E. and Bowman, F. M.: Estimated Effects of Temperature on Secondary Organic Aerosol
789 Concentrations, *Environ. Sci. Technol.*, 35, 2129-2135, 10.1021/es001547g, 2001.

790 Shiraiwa, M., Ammann, M., Koop, T., and Pöschl, U.: Gas uptake and chemical aging of semisolid
791 organic aerosol particles, *Proc. Natl. Acad. Sci.*, 108, 11003-11008, doi:10.1073/pnas.1103045108,
792 2011.

793 Shiraiwa, M., Li, Y., Tsimpidi, A. P., Karydis, V. A., Berkemeier, T., Pandis, S. N., Lelieveld, J., Koop, T.,
794 and Pöschl, U.: Global distribution of particle phase state in atmospheric secondary organic aerosols,
795 *Nat. Commun.*, 8, 15002, 10.1038/ncomms15002, 2017.

796 Simon, M., Dada, L., Heinritzi, M., Scholz, W., Stolzenburg, D., Fischer, L., Wagner, A. C., Kürten, A.,
797 Rörup, B., He, X. C., Almeida, J., Baalbaki, R., Baccarini, A., Bauer, P. S., Beck, L., Bergen, A., Bianchi, F.,
798 Bräkling, S., Brilke, S., Caudillo, L., Chen, D., Chu, B., Dias, A., Draper, D. C., Duplissy, J., El-Haddad, I.,
799 Finkenzeller, H., Frege, C., Gonzalez-Carracedo, L., Gordon, H., Granzin, M., Hakala, J., Hofbauer, V.,
800 Hoyle, C. R., Kim, C., Kong, W., Lamkaddam, H., Lee, C. P., Lehtipalo, K., Leiminger, M., Mai, H.,
801 Manninen, H. E., Marie, G., Marten, R., Mentler, B., Molteni, U., Nichman, L., Nie, W., Ojdanic, A.,
802 Onnela, A., Partoll, E., Petäjä, T., Pfeifer, J., Philippov, M., Quéléver, L. L. J., Ranjithkumar, A., Rissanen,
803 M. P., Schallhart, S., Schobesberger, S., Schuchmann, S., Shen, J., Sipilä, M., Steiner, G., Stozhkov, Y.,



804 Tauber, C., Tham, Y. J., Tomé, A. R., Vazquez-Pufleau, M., Vogel, A. L., Wagner, R., Wang, M., Wang, D.
805 S., Wang, Y., Weber, S. K., Wu, Y., Xiao, M., Yan, C., Ye, P., Ye, Q., Zauner-Wieczorek, M., Zhou, X.,
806 Baltensperger, U., Dommen, J., Flagan, R. C., Hansel, A., Kulmala, M., Volkamer, R., Winkler, P. M.,
807 Worsnop, D. R., Donahue, N. M., Kirkby, J., and Curtius, J.: Molecular understanding of new-particle
808 formation from α -pinene between -50 and +25 °C, *Atmos. Chem. Phys.*, 20, 9183-9207, 10.5194/acp-
809 20-9183-2020, 2020.
810 Sindelarova, K., Granier, C., Bouarar, I., Guenther, A., Tilmes, S., Stavrakou, T., Müller, J. F., Kuhn, U.,
811 Stefani, P., and Knorr, W.: Global data set of biogenic VOC emissions calculated by the MEGAN model
812 over the last 30 years, *Atmos. Chem. Phys.*, 14, 9317-9341, 10.5194/acp-14-9317-2014, 2014.
813 Sofiev, M., Vankevich, R., Lanne, M., Koskinen, J., and Kukkonen, J.: On Integration Of A Fire
814 Assimilation System And A Chemical Transport Model For Near-realtime Monitoring Of The Impact Of
815 Wild-land Fires On Atmospheric Composition And Air Quality, *WIT Trans. Ecol. Environ.*, 119, 343-351,
816 2008.
817 Stark, H., Yatavelli, R. L. N., Thompson, S. L., Kang, H., Krechmer, J. E., Kimmel, J. R., Palm, B. B., Hu, W.,
818 Hayes, P. L., Day, D. A., Campuzano-Jost, P., Canagaratna, M. R., Jayne, J. T., Worsnop, D. R., and
819 Jimenez, J. L.: Impact of Thermal Decomposition on Thermal Desorption Instruments: Advantage of
820 Thermogram Analysis for Quantifying Volatility Distributions of Organic Species, *Environmental
821 Science & Technology*, 51, 8491-8500, 10.1021/acs.est.7b00160, 2017.
822 Surdu, M., Top, J., Yang, B., Zhang, J., Slowik, J. G., Prévôt, A. S. H., Wang, D. S., el Haddad, I., and Bell,
823 D. M.: Real-Time Identification of Aerosol-Phase Carboxylic Acid Production Using Extractive
824 Electrospray Ionization Mass Spectrometry, *Environmental Science & Technology*, 58, 8857-8866,
825 10.1021/acs.est.4c01605, 2024.
826 Takeuchi, M., Berkemeier, T., Eris, G., and Ng, N. L.: Non-linear effects of secondary organic aerosol
827 formation and properties in multi-precursor systems, *Nat. Commun.*, 13, 7883, 10.1038/s41467-022-
828 35546-1, 2022.
829 Tripathi, N., Krumm, B. E., Edtbauer, A., Ringsdorf, A., Wang, N., Kohl, M., Vella, R., Machado, L. A. T.,
830 Pozzer, A., Lelieveld, J., and Williams, J.: Impacts of convection, chemistry, and forest clearing on
831 biogenic volatile organic compounds over the Amazon, *Nature Communications*, 16, 4692,
832 10.1038/s41467-025-59953-2, 2025.
833 Trump, E. R. and Donahue, N. M.: Oligomer formation within secondary organic aerosols: equilibrium
834 and dynamic considerations, *Atmos. Chem. Phys.*, 14, 3691-3701, 10.5194/acp-14-3691-2014, 2014.
835 Tsimpidi, A. P., Karydis, V. A., Zavala, M., Lei, W., Molina, L., Ulbrich, I. M., Jimenez, J. L., and Pandis, S.
836 N.: Evaluation of the volatility basis-set approach for the simulation of organic aerosol formation in the
837 Mexico City metropolitan area, *Atmos. Chem. Phys.*, 10, 525-546, 10.5194/acp-10-525-2010, 2010.
838 Vallon, M., Gao, L., Jiang, F., Krumm, B., Nadolny, J., Song, J., Leisner, T., and Saathoff, H.: LED-based
839 solar simulator to study photochemistry over a wide temperature range in the large simulation
840 chamber AIDA, *Atmos. Meas. Tech.*, 15, 1795-1810, 10.5194/amt-15-1795-2022, 2022.
841 Visschedijk, A., Zandveld, P., and Denier Van Der Gon, H.: A high resolution gridded European emission
842 database for the EU integrated project GEMS, TNO report, 2007.
843 Wagner, R., Bunz, H., Linke, C., Möhler, O., Naumann, K.-H., Saathoff, H., Schnaiter, M., and Schurath,
844 U.: Chamber Simulations of Cloud Chemistry: The AIDA Chamber, Environmental Simulation Chambers:
845 Application to Atmospheric Chemical Processes, Dordrecht, 2006//, 67-82,
846 Wang, Y., Zhao, Y., Li, Z., Li, C., Yan, N., and Xiao, H.: Importance of Hydroxyl Radical Chemistry in
847 Isoprene Suppression of Particle Formation from α -Pinene Ozonolysis, *ACS Earth Space Chem.*, 5, 487-
848 499, 10.1021/acsearthspacechem.0c00294, 2021.
849 Xu, L., Kollman, M. S., Song, C., Shilling, J. E., and Ng, N. L.: Effects of NOx on the Volatility of Secondary
850 Organic Aerosol from Isoprene Photooxidation, *Environ. Sci. Technol.*, 48, 2253-2262,
851 10.1021/es404842g, 2014.
852 Yáñez-Serrano, A. M., Nölscher, A. C., Bourtsoukidis, E., Gomes Alves, E., Ganzeveld, L., Bonn, B., Wolff,
853 S., Sa, M., Yamasoe, M., Williams, J., Andreae, M. O., and Kesselmeier, J.: Monoterpene chemical



854 speciation in a tropical rainforest: variation with season, height, and time of day at the Amazon Tall
855 Tower Observatory (ATTO), *Atmos. Chem. Phys.*, 18, 3403-3418, 10.5194/acp-18-3403-2018, 2018.
856 Yáñez-Serrano, A. M., Bourtsoukidis, E., Alves, E. G., Bauwens, M., Stavrakou, T., Llusia, J., Filella, I.,
857 Guenther, A., Williams, J., Artaxo, P., Sindelarova, K., Doubalova, J., Kesselmeier, J., and Peñuelas, J.:
858 Amazonian biogenic volatile organic compounds under global change, *Global Change Biology*, 26,
859 4722-4751, <https://doi.org/10.1111/gcb.15185>, 2020.
860 Ye, Q., Wang, M., Hofbauer, V., Stolzenburg, D., Chen, D., Schervish, M., Vogel, A., Mauldin, R. L.,
861 Baalbaki, R., Brilke, S., Dada, L., Dias, A., Duplissy, J., El Haddad, I., Finkenzeller, H., Fischer, L., He, X.,
862 Kim, C., Kürten, A., Lamkaddam, H., Lee, C. P., Lehtipalo, K., Leiminger, M., Manninen, H. E., Marten,
863 R., Mentler, B., Partoll, E., Petäjä, T., Rissanen, M., Schobesberger, S., Schuchmann, S., Simon, M., Tham,
864 Y. J., Vazquez-Pufleau, M., Wagner, A. C., Wang, Y., Wu, Y., Xiao, M., Baltensperger, U., Curtius, J.,
865 Flagan, R., Kirkby, J., Kulmala, M., Volkamer, R., Winkler, P. M., Worsnop, D., and Donahue, N. M.:
866 Molecular Composition and Volatility of Nucleated Particles from α -Pinene Oxidation between -50 °C
867 and $+25$ °C, *Environmental Science & Technology*, 53, 12357-12365, 10.1021/acs.est.9b03265, 2019.
868 Zhang, X., McVay, R. C., Huang, D. D., Dalleska, N. F., Aumont, B., Flagan, R. C., and Seinfeld, J. H.:
869 Formation and evolution of molecular products in α -pinene secondary organic aerosol, *Proc. Natl. Acad.
870 Sci.*, 112, 14168-14173, doi:10.1073/pnas.1517742112, 2015.
871